AIAA JOURNAL
Vol. 40, No. 8, August 2002

Deforming Mesh for Computational Aeroelasticity Using a Nonlinear Elastic Boundary Element Method

Xiao-Wei Gao,* Ping-Chih Chen,† and Lei Tang‡
ZONA Technology, Inc., Scottsdale, Arizona 85251

A nonlinear elastic boundary element method (NBEM) approach is developed as an innovative deforming mesh generator for computational aeroelastic simulation. The computational fluid dynamics (CFD) mesh is assumed to be embedded in an infinite nonlinear elastic medium of a hardening material, leading to the formulation of a pseudononlinear elastostatic problem. Whereas the CFD surface mesh is treated as a boundary element model and the CFD flowfield grid as domain sample points, the NBEM approach solves Navier's equations using a particular solution scheme that removes the requirement of the domain integral in the conventional NBEM formulation. The NBEM approach has a unified feature that is applicable to all mesh systems, including unstructured, multiblock structured, and overset grids. An optimization strategy is employed to determine the optimum hardening material properties by minimizing the mesh distortion in the viscous region where grid orthogonality must be preserved. Three test cases are performed to demonstrate the robustness and effectiveness of the NBEM approach for deforming mesh generation.

Introduction

DURING the past two decades, research on the application of computational fluid dynamics (CFD) methods to aeroelastic analysis has been rapidly progressing. To date, implicit Navier–Stokes algorithms with the geometric conservation law and Newton-like subiterations for time-accurate aeroelastic simulation of three-dimensional elastic bodies have been well established.[1–3] Production-ready computer codes such as CFL3D (Ref. 4), ENS3DAE (Refs. 5 and 6), and ENSAERO (Ref. 7) are nearly completed and available to the U.S. aerospace industry. However, application of these CFD codes on complex configurations such as a whole aircraft with external stores or nacelles is still hampered by the lack of a robust and efficient deforming mesh algorithm. In general, there are two technical issues involved in the deforming mesh algorithm for CFD aeroelastic simulations: 1) data transferal between the structural finite element (FEM) grid and CFD surface grid and 2) deforming the CFD flowfield grid.

Data Transferal Between the Structural FEM Grid and the CFD Surface Grid

Here, the CFD surface grid is defined as the mesh on the surface of the bodies where the moving boundary condition is imposed. Because the CFD surface grid and the structural FEM grid could be considerably different, the aeroelastic computation requires the data transferal between these two grid systems. This technical issue usually involves the transferal of displacements computed at the FEM grid to the CFD surface grid and the transferal of loads computed at the CFD surface grid back to the FEM grid.

Deforming the CFD Flowfield Grid

Once the displacements at the CFD surface grid are obtained from the FEM grid by the data transferal methodology just discussed, the CFD deformed flowfield grid must conform to the deformed CFD surface grid by a deforming flowfield grid algorithm. In the time-marching aeroelastic simulation, this deformed flowfield grid must be updated at every time level according to the instantaneous deformed CFD surface grid positions. These deformed CFD flowfield grids should satisfy four basic requirements:

1) No grid line crossover may occur to ensure the positivity of the cell volume.

2) The grid orthogonality must be, at least nearly, preserved. It is important to ensure such orthogonality in the viscous region near the surface grid.

3) The transition of the deformation from that of the surface grid to the zero deformation in the far-field grid should be kept as smooth as possible.

4) The clustering of the near-body grid cannot be compromised as the body deforms. The grid must maintain its clustering in the viscous layer.

Using an innovative structural boundary element method (BEM), Chen and Jadic[8] and Chen and Hill[9] have developed a data transformation technique, called the BEM solver, that generates a universal spline matrix to relate directly the displacements and loads between the CFD structural grid and the FEM grid. During the development of the BEM solver, it was realized that the BEM can also be employed as a deforming flowfield grid algorithm. This can be achieved by assuming the flowfield grid to be embedded in an infinite nonlinear elastic medium of a hardening material. In this paper, we will focus on the discussion of such an approach for deforming flowfield grid generation. Results of three test cases using such an approach are also shown to demonstrate its robustness and applicability for CFD computations.

Review of Existing Deforming Grid Algorithms

There are generally two kinds of approaches to generate deforming grids: the algebraic method and the pseudostructural method. The most commonly used algebraic method is the transfinite interpolation (TFI) scheme with the mesh orthogonality constraint at the deforming surface.[10] The TFI scheme offers an efficient deforming grid algorithm for structured meshes, but it would be difficult to apply TFI on an unstructured mesh. Also, an extension of the TFI scheme to a multiblock structured mesh for a complex configuration is by no means a trivial task.

The spring analogy scheme, first developed by Batina,[11] belongs to the pseudo-structural methods that model the mesh as a network of lineal springs and solve the static equilibrium equations for this network to determine the new locations of the grid points. Farhat et al.[12] proposed a modified spring analogy by adding additional nonlinear torsion springs to avoid the nonpositive cell volume problem associated with the lineal spring network. By the use of a hybrid spring

Received 18 August 2000; revision received 25 January 2002; accepted for publication 12 February 2002.

*Engineering Specialist, 7430 East Stetson Drive, Suite 205; gao@zonatech.com.

†Vice President, 7430 East Stetson Drive, Suite 205; pc@zonatech.com. Member AIAA.

‡Computational Fluid Dynamics Specialist, 7430 East Stetson Drive, Suite 205; tangl@zonatech.com. Member AIAA.

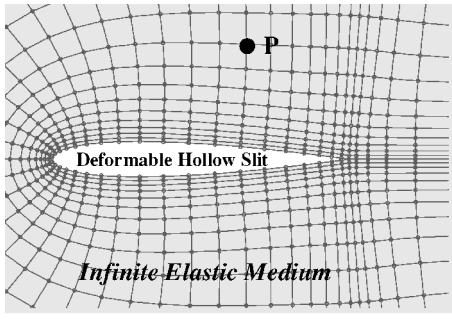

Fig. 1 BEM for deforming flowfield grid.

analogy-TFI approach, Bartels[13] has shown a two-dimensional deforming one-block structured mesh for an oscillating spoiler study. Because the numerical technique for solving the deformation of the spring network is essentially the structural FEM that inherently requires an unstructured grid, the spring analogy scheme can be directly applied to generate the deforming grid of the unstructured mesh. On the other hand, because the structural FEM does not allow grid mismatch between adjacent elements, the application of the spring analogy scheme on a multiblock structured mesh with grid mismatch on the block interfaces would be difficult. Based on the same reason, it is obvious that the application of the spring analogy on an overset mesh is not feasible.

Based on the preceding discussion, it is concluded that neither the TFI technique nor the spring analogy scheme can be generalized to deal with any given mesh system, that is, unstructured, multiblock structured, and overset grids. By the use of a linear boundary element method, Chen and Jadic[8] developed an exterior BEM solver that has a unified feature for the deforming flowfield grid generation of all grid systems. When it is assumed that the CFD mesh is to be embedded in an infinite linear elastic medium where the CFD surface grid is treated as a deformable hollow slit (Fig. 1), a pseudoelastostatic problem with an infinite elastic domain can be formulated. This is a perfect boundary element problem because BEM only requires modeling the surface of the body and, therefore, is ideally suitable for dealing with the infinite elastic domain.

The starting point for the derivation of the pseudoelastostatic BEM equations are Navier's (equilibrium) equations in terms of displacement u_i, which in tensor notation have the form

$$Gu_{i,jj} + (G + \lambda)u_{j,ji} = 0 \tag{1}$$

where λ is the Láme coefficient and G is the shear modulus.

The BEM is based on the boundary integral equations of Navier's equations. The result is known as Somigliana's identity that relates the displacement at any point p (Fig. 1) to the displacement u_s and tractions t_s on the boundary, that is,

$$u_i(p) = \int_\Gamma u^*_{is} t_s \, d\Gamma - \int_\Gamma t^*_{is} u_s \, d\Gamma \tag{2}$$

where u^*_{is} and t^*_{is} are the Kelvin kernels of the displacement and traction, respectively, and Γ denotes the boundary of the body. When the CFD surface grid points are connected with the boundary elements to form a discretized BEM model, Eq. (2) can be recast into the following matrix form:

$$u(p) = \boldsymbol{G}_{sp} t_s - \boldsymbol{H}_{sp} u_s \tag{3}$$

where $\boldsymbol{G}_{sp}$ and $\boldsymbol{H}_{sp}$ are the so-called traction and displacement coefficient matrices, respectively, and the subscripts sp refer to the surface-to-flowfield point influence.

A special treatment of the boundary integral equation (2) is required for points on the boundary. In matrix form, the equation that relates the displacement u_s and traction t_s on the boundary is

$$\boldsymbol{H}_{ss} u_s = \boldsymbol{G}_{ss} t_s \tag{4}$$

where the subscripts ss refers to the surface-to-surface influence.

Substituting Eq. (4) into Eq. (3) yields the exterior BEM solver that reads

$$u(p) = \boldsymbol{B} u_s \tag{5}$$

where

$$\boldsymbol{B} = \boldsymbol{G}_{sp} \boldsymbol{G}^{-1}_{ss} \boldsymbol{H}_{ss} - \boldsymbol{H}_{sp} \tag{6}$$

Note that the matrix $\boldsymbol{B}$ is independent of the deformation u_s and invariant during the time-marching aeroelastic computation because it is evaluated on the undeformed mesh. Also, because the point p can be assigned anywhere in the flowfield, the generation of matrix $\boldsymbol{B}$ does not require the connectivity information of the flowfield grid points and, therefore, is independent of the mesh system. Thus, the exterior BEM solver offers several technical merits over the spring analogy scheme as follows:

1) It can be generalized to deal with all grid systems.

2) Because the computation of $u(p)$ is a point-by-point procedure, it can be easily parallelized.

3) Because the elastostatic formulation of BEM involves both the volume modulus (equivalent to the lineal spring) and the shear modulus (equivalent to the torsion spring) of a continuous elastic medium, the transition of the grid deformation is always smooth.

4) The zero deformation requirement in the far-field grid is inherently satisfied because of the infinite elastic medium characteristics.

However, for problems with a relatively large mesh motion amplitude, the exterior BEM solver suffers from the shortcoming of the linear elastic assumption. An example of this is shown in Figs. 2 and 3. Figure 2 shows a given undeformed viscous mesh of a NACA 0012 airfoil. By the imposition of a 20-deg pitch-up angle about the

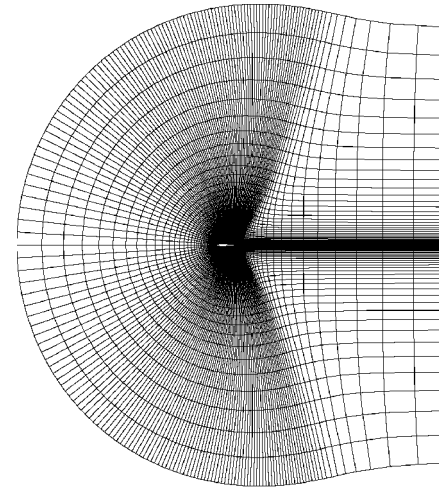

Fig. 2 Given undeformed mesh of NACA 0012 airfoil.

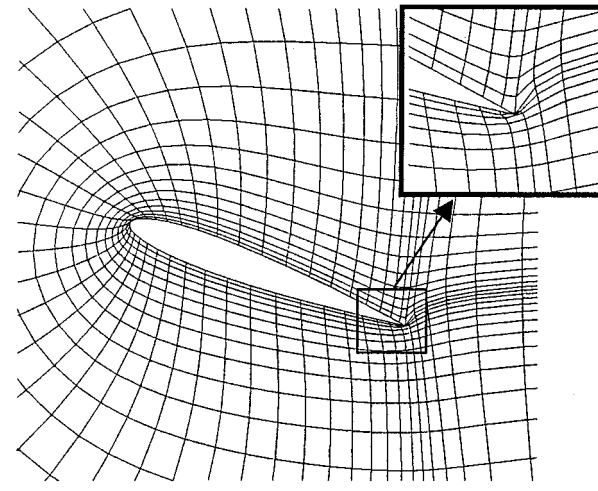

Fig. 3 Unacceptable deformed mesh by the linear exterior BEM solver.

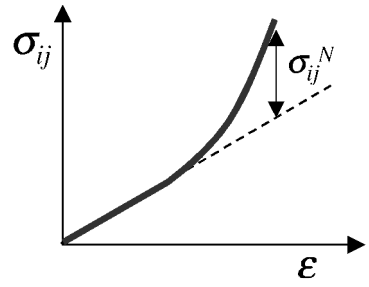

Fig. 4 Stress (σ_{ij})–strain (ε) relationship of hardening material.

50% chord, the resulting deformed mesh using the exterior BEM solver is depicted in Fig. 3. (For clarity, only a coarse deformed mesh is shown.) A large distortion of the mesh to the extent that grid line crossover occurs near the leading and trailing edges can be seen. Also, the grid orthogonality in the viscous region is destroyed. Because the imposed displacement occurs on the surface mesh only, large elastic stresses are concentrated near the surface and decay rapidly toward the far field. Because of the linear elastic assumption, a large stress can induce a large strain, implying large distortion of the mesh in the high-stress region.

To overcome this problem, it is apparent that a nonlinear elastic medium of hardening material must be employed. A typical stress–strain relationship of the hardening material is shown in Fig. 4. Within this hardening material, high stress will not necessarily yield high strain, thereby reducing the mesh distortion in the high-stress region. However, solving the elastostatic problem with hardening material requires a nonlinear elastic BEM approach.

Nonlinear Elastic BEM Formulation

In nonlinear elastic BEM for strain hardening materials, the stress is no longer the linear response to the strain, and the quantities are usually expressed in incremental forms. With reference to Fig. 4, the stress increment can be decomposed into two parts, as follows

$$\dot{\sigma}_{ij} = \dot{\sigma}^e_{ij} + \dot{\sigma}^N_{ij} \tag{7}$$

where the over dot indicates that it is an increment and $\dot{\sigma}^e_{ij}$ is the linear part, which is determined by Hook's law as

$$\dot{\sigma}^e_{ij} = G D_{ijkl} \dot{\varepsilon}_{kl} \tag{8}$$

$$D_{ijkl} = [2\nu/(1-2\nu)]\delta_{ij}\delta_{kl} + \delta_{ik}\delta_{jl} + \delta_{il}\delta_{jk} \tag{9}$$

in which ν is the Poisson ratio, G is the shear modulus, and $\dot{\varepsilon}_{kl}$ is the strain increment.

The nonlinear stress increment $\dot{\sigma}^N_{ij}$ is assumed to have the similar relationship to Eq. (8), but the shear modulus is a function of strain, that is,

$$\dot{\sigma}^N_{ij} = GG'(J_1, J_2) D_{ijkl} \dot{\varepsilon}_{kl} = G'(J_1, J_2)\dot{\sigma}^e_{ij} \tag{10}$$

To minimize the mesh distortion, the high-stress region near the surface mesh suggests that $G'(J_1, J_2)$ should represent a strongly hardening function of strain. Such a function is expressed as follows:

$$G'(J_1, J_2) = e^{\alpha J_1 + \beta J_2} \tag{11}$$

Here, α and β are weighting factors to measure the contributions of the effective volume strain J_1 and the shear strain J_2 to the hardening behavior of $G'(J_1, J_2)$. J_1 and J_2 are the first and second invariants of the strain tensor and the deviatorical strain tensor, respectively, which are defined as

$$J_1 = (\varepsilon_{kk})^2 \tag{12}$$

$$J_2 = \tfrac{1}{2}\varepsilon'_{ij}\varepsilon'_{ij} \tag{13}$$

where ε'_{ij} is the deviatorical tensor

$$\varepsilon'_{ij} = \varepsilon_{ij} - \tfrac{1}{3}\varepsilon_{kk}\delta_{ij} \tag{14}$$

J_1 and J_2 are related to volume and shear strains, respectively.

Navier's equations with the nonlinear stress $\dot{\sigma}^N_{ij}$ can be written as

$$G\dot{u}_{i,jj} + (G+\lambda)\dot{u}_{j,ji} = -\dot{\sigma}^N_{ij,j} \tag{15}$$

In the conventional nonlinear BEM formulation, the integral boundary equations for Navier's equation (15) involve a domain integral of the nonlinear stress. The computations of this domain integral require the discretization of the problem domain into volume cells. This destroys one of the major advantages of adopting the BEM as a mesh-system independent algorithm. Banerjee and Henry[14] proposed a particular solution scheme that removes the requirement of the volume cells. This particular solution scheme assumes that the solutions of Eq. (15) consist of two parts, that is,

$$\dot{u}_i = \dot{u}^c_i + \dot{u}^p_i \tag{16}$$

where $\dot{u}^c_i$ is referred to as the complementary solution, which satisfies the homogeneous Navier's equations (1), and can be obtained from the linear BEM equations described in the preceding section. The displacement $\dot{u}^p_i$ in Eq. (16) is referred to as the particular solutions, which satisfies Eq. (15).

Before solution, the distribution of the nonlinear stresses $\dot{\sigma}^N_{ij}$ are unknown. We assume that $\dot{\sigma}^N_{ij}$ can be derived from a biharmonic function $\dot{h}_{ij}$, that is,

$$\dot{\sigma}^N_{ij} = -\dot{h}_{ij,mmnn} \tag{17}$$

Based on this assumption, the displacement particular solution can be found[15] as

$$\dot{u}^p_i = (1/G)\dot{h}_{ij,jkk} - [1/2G(1-\nu)]\dot{h}_{kj,jki} \tag{18}$$

From Eqs. (17) and (18), we can see that, once we know the distribution of $\dot{h}_{ij}$, the particular solutions for nonlinear stresses and displacements can be determined. To achieve this, a global shape function $C(x, d_n)$ (Ref. 14) is used for interpolation of $\dot{h}_{ij}$, as follows:

$$\dot{h}_{ij}(x) = \sum_{n=1}^{N} C(x, d_n)\dot{\phi}_{ij}(d_n) \tag{19}$$

where $\dot{\phi}_{ij}$ are constants to be determined and

$$C(x, d_n) = A(\rho^4 - b\rho^5) \tag{20}$$

Here, A is generally taken as the fourth power of some characteristic length associated with the BEM model, b can generally be set equal to unity, and ρ is the distance between x and d_n. Usually, d_n are chosen to be the boundary nodes and some sample points in the domain.

By substituting Eq. (19) into Eqs. (17) and (18), and with the results being written in matrix form, we have

$$\dot{\sigma}^N = \boldsymbol{K}\dot{\phi} \tag{21}$$

$$\dot{u}^p = \boldsymbol{D}\dot{\phi} \tag{22}$$

in which $\boldsymbol{K}$ is a diagonal matrix and $\dot{\phi}$ is a vector of $\dot{\phi}_{ij}$ at all sample points. The elements are

$$k(x, d_n) = C(x, d_n)_{,kkll} = A(120 - 360b\rho) \tag{23}$$

The matrix $\boldsymbol{D}$ in Eq. (22) is formed from the following expression:

$$d_{ijk}(x, d_n) = (1/G)C(x, d_n)_{,jll}\delta_{ik} - [1/2G(1-\nu)]C(x, d_n)_{,jki} \tag{24}$$

Note that the matrix $\boldsymbol{K}$ in Eq. (21) is invertible, and so the vector $\dot{\phi}$ can be expressed in terms of the vector $\dot{\sigma}^N$. With this in mind, and using the preceding linear BEM equations together with Eqs. (7), (16), (21), and (22), the nonlinear BEM equations (in matrix form) can be formed as follows:

$$\boldsymbol{A}^b\dot{X} = \dot{Y}^b + \boldsymbol{E}^b\dot{\sigma}^N \tag{25}$$

$$\dot{\sigma} = \boldsymbol{A}^x\dot{X} + \dot{Y}^\sigma + \boldsymbol{E}^\sigma\dot{\sigma}^N \tag{26}$$

where $\boldsymbol{A}^b$ and $\boldsymbol{A}^x$ are coefficient matrices formed by boundary integrals and $\boldsymbol{E}^b$ and $\boldsymbol{E}^\sigma$ are nonlinear coefficient matrices formed by global functions. Note that Eqs. (25) and (26) are very similar to those derived for elastic–plastic problems[16] where the matrices $\boldsymbol{E}^b$ and $\boldsymbol{E}^\sigma$ are formed by domain integration.

Combining Eqs. (7), (10), (25), and (26) yields

$$\boldsymbol{A}\dot{\sigma}^e = \dot{Y} \tag{27}$$

where

$$\boldsymbol{A} = \boldsymbol{I} + \left(\boldsymbol{I} - \boldsymbol{E}^\sigma - \boldsymbol{A}^x \boldsymbol{A}^{b^{-1}} \boldsymbol{E}^b\right)\boldsymbol{G}' \tag{28}$$

$$\dot{Y} = \dot{Y}^\sigma + \boldsymbol{A}^x \boldsymbol{A}^{b^{-1}} \dot{Y}^b \tag{29}$$

The system of Eqs. (27) is a nonlinear equation set because the coefficient matrix $\boldsymbol{A}$ is the function of strains. The standard Newton–Raphson iterative scheme[16] can be used to solve this equation set. Close inspection of Eq. (28) shows that only the matrix $\boldsymbol{G}'$, which is a diagonal matrix and formed from Eq. (11), is the function of strains. Therefore, quick convergence can be achieved in the iteration procedure.

The particular solution scheme described for solving the nonlinear Navier's equation is an ideal solution scheme for CFD deforming grid generation. Only the CFD flowfield grids are used as sample points in the domain, thereby removing the need of connectivity information of the CFD mesh system. For large-amplitude surface deformation, the computational procedure involves an incremental process that solves the unknown boundary traction and also builds up information about the incremental solutions at the domain sample points.

Optimization for Optimum Hardening Material Properties

Because the present NBEM approach is based on a pseudoelastostatic formulation, the hardening behavior of the elastic medium (shown in Fig. 1) dominates the quality of the deformed mesh. To determine automatically the optimum hardening material properties, we use an optimization procedure to search for the best values of α and β in Eq. (11). The key issue in formulating such an optimization procedure is how to define an objective function that can relate the quality of the deformed mesh to the design variables, namely, α and β. Because minimum strain is equivalent to minimum mesh distortion, the objective function to be minimized in the optimization procedure is defined as

$$f(\alpha, \beta) = \sum_{l=1}^{n} (\varepsilon_{ij}\varepsilon_{ij})_l \tag{30}$$

where f is the objective function, ε_{ij} is the strain tensor at grid l, and n is the number of grid points where the strain tensor ε_{ij} is evaluated. These grid points are selected like those in the viscous region, where preserving the grid orthogonality is important.

Test Cases and Discussion

Three two-dimensional test cases are selected to demonstrate the robustness and effectiveness of the NBEM approach. CFD computations using the deformed mesh generated by the NBEM are performed, and the resulting pressure distributions are used to assess the quality of the deformed mesh.

Case 1: NACA 0012 Airfoil at 20-Degree Pitch-Up Angle at About 50% Chord

For a given undeformed mesh of a NACA 0012 airfoil (Fig. 2), a surface deformation corresponding to a 20-deg pitch-up angle about the 50% chord is imposed on the surface mesh. The overall deformed mesh computed by the NBEM approach is shown in Fig. 5a. As expected, the far-field mesh is practically undeformed because of the characteristics of the infinite elastic medium. The zoomed-in view of the deformed mesh near the airfoil surface depicted in Fig. 5b clearly shows the smooth transition of the deformation from the surface mesh to the far-field mesh. For clarity, the deformed mesh near the leading and trailing edges is further expanded and shown in Figs. 5c–5f. Note that the orthogonality of the deformed mesh in the viscous region is preserved. The transition of the deformed mesh from the trailing edge to the wake region appears to be smooth, forming a curved wake surface grid whose deformation decays rapidly from the trailing edge to downstream.

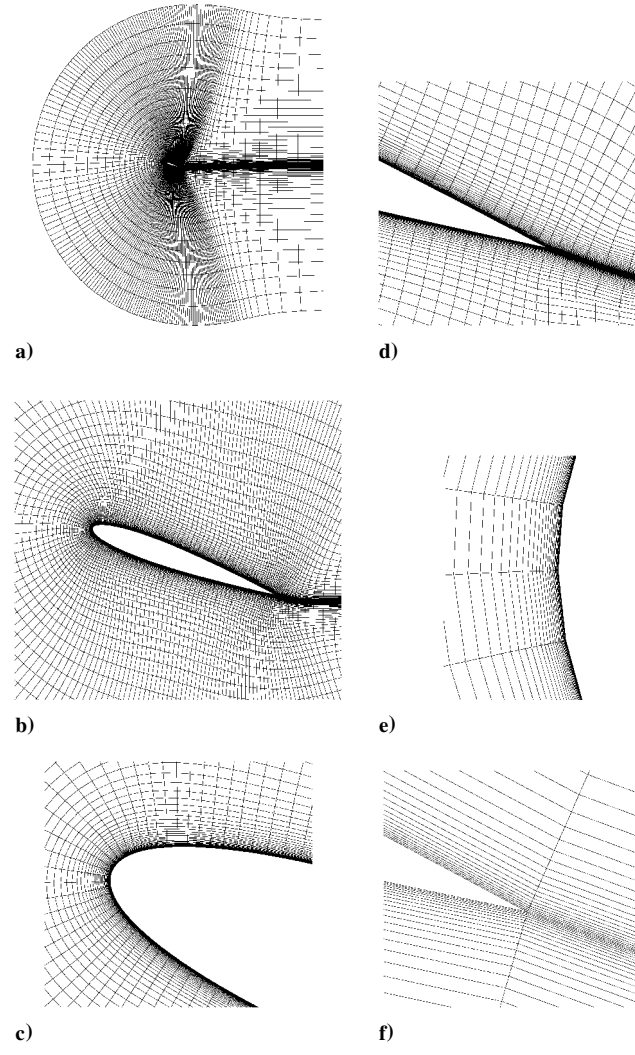

Fig. 5 Deformed mesh of NACA 0012 airfoil section at 20-deg pitch-up angle at about 50% chord.

In theory, the CFD result of a deformed mesh at 20-deg pitch-up angle and 0-deg angle of attack (AOA) ($\theta = 20$ deg, AOA $= 0$ deg) should be the same as that of the corresponding undeformed mesh at $\theta = 0$ deg and AOA $= 20$ deg if the deformed mesh is of good quality. To verify this, two Navier–Stokes computations using the CFL3D code with the Spalart–Allmaras model were performed at $M = 0.7$ and $Re = 2.0 \times 10^5$, one on the deformed mesh at AOA $= 0$ deg and the second one on the undeformed mesh at AOA $= 20$ deg. Excellent agreement of the surface pressure, C_P, distributions for these two meshes is obtained and shown in Fig. 6. Note that at a 20-deg incidence angle, the NACA 0012 is already beyond its stall AOA. This is to say that the behavior of the separated flow on the upper surface of the airfoil is very sensitive to the quality of the mesh, particularly at the leading edge. The excellent agreement of the C_P shown in Fig. 6 clearly demonstrates the capability of the NBEM approach for high-quality deforming grid generation in terms of the smoothness and orthogonality of the mesh.

Case 2: NACA 0012 Airfoil at 10-Degree Trailing-Edge Flap Deflection Angle

Control surface deflection creates a discontinuity in slope across the hinge. For the pseudostructural method like the spring analogy, this gives a stress concentration around the hinge that may destroy the quality of the deformed mesh. To show that this is not the case for the NBEM approach, a 10-deg trailing-edge flap deflection angle with hinge at the 75% chord of the NACA 0012 airfoil is imposed on the surface mesh. Figure 7 shows the NBEM computed deformed mesh where the smoothness and the near-surface orthogonality of

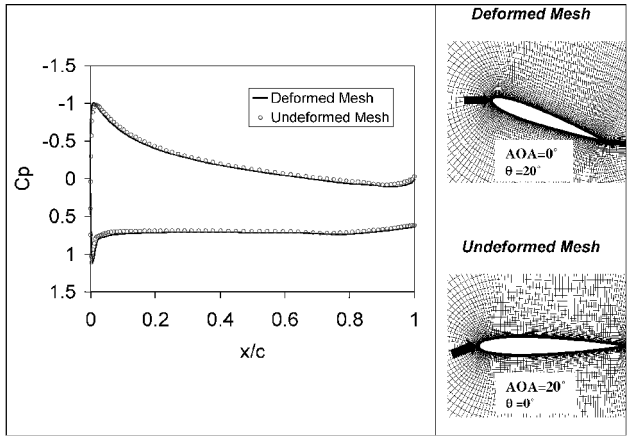

Fig. 6 Steady pressure of deformed and undeformed mesh of NACA 0012 airfoil section at 20-deg pitch-up angle at about 50% chord, Mach 0.7, and $Re = 2.0 \times 10^5$.

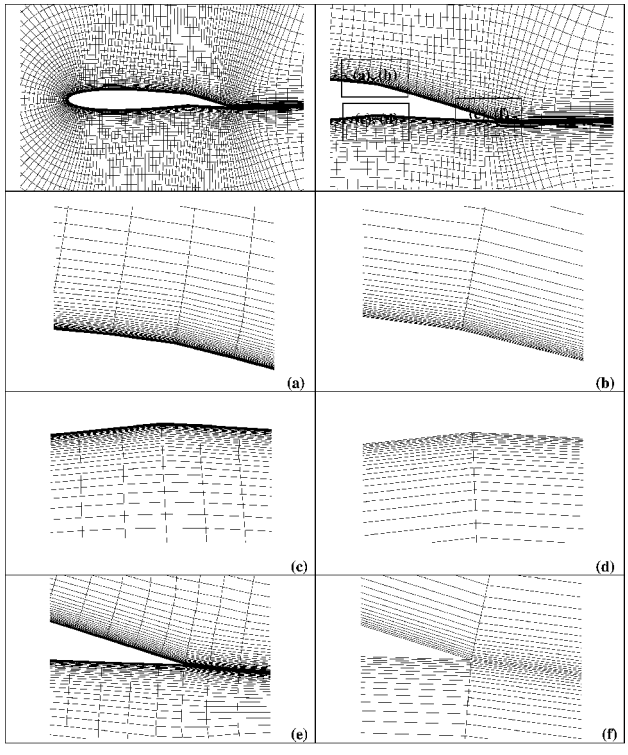

Fig. 7 Deformed mesh of NACA 0012 airfoil section with a 10-deg trailing-edge flap with deflection angle.

the deformation can be clearly seen. The C_P distribution of this deformed mesh (Fig. 8) computed by the CFL3D code at $M = 0.7$, AOA $= 0$ deg, and $Re = 2.0 \times 10^6$ shows a spike on the upper surface at the hinge location due to the slope discontinuity. This expected spike indicates that the slope discontinuity at the hinge is well captured by the NBEM approach.

Case 3: Mesh Morphing from NACA 0016 Airfoil to NLR 7301 Airfoil

Changing the surface mesh to obtain a conforming mesh according to the new surface, but without directly using a grid generator, is defined here as mesh morphing. Mesh morphing is an essential element involved in aerodynamic optimization using CFD methods because it is an automated procedure and can provide an updated mesh at each design cycle. To show that the NBEM approach can be used for mesh morphing, a given mesh of a conventional NACA 0016 airfoil is deformed to yield a mesh for the supercritical National Aerospace Laboratory (NLR) 7301 airfoil. Figure 9 shows the surface geometry of the NACA 0016 and NLR 7301 airfoils.

The difference between these two surfaces is the grid movement imposed onto the NACA 0016 surface mesh, rendering a deformed

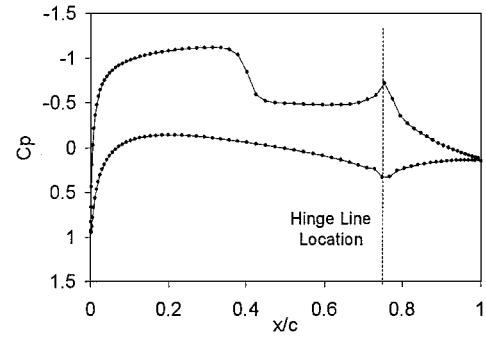

Fig. 8 Pressure distribution of NACA 0012 with 10-deg trailing-edge flap deflection angle, Mach 0.7, AOA = 0 deg, and $Re = 2.0 \times 10^6$.

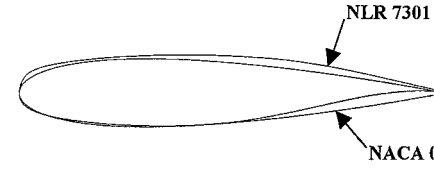

Fig. 9 Surface grid movement from NACA 0016 to NLR 7301 airfoil.

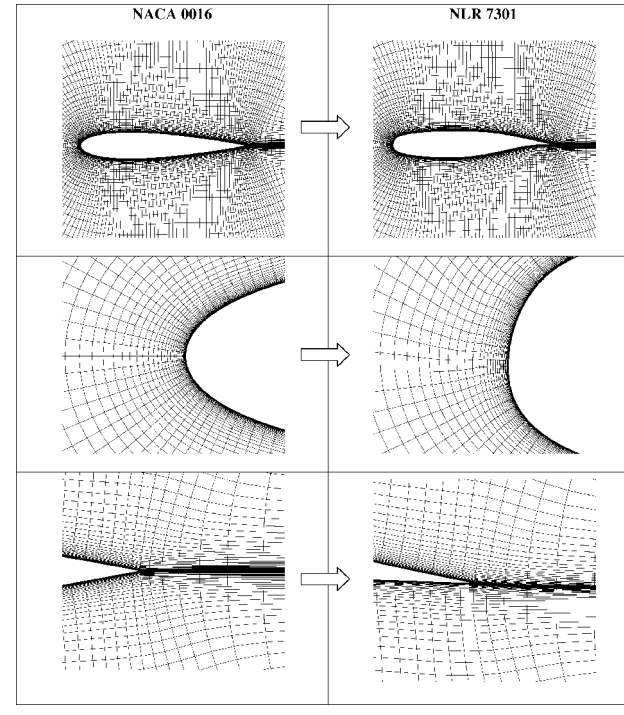

Fig. 10 Mesh morphing from NACA 0016 airfoil to NLR 7301 airfoil.

flowfield mesh. Such a deformed mesh computed by the NBEM approach is shown in Fig. 10a that corresponds to a mesh system for the NLR 7301 airfoil. The given mesh for the NACA 0016 airfoil is also shown, in Fig. 10b. The difference between these two meshes is the grid deformation computed by the NBEM approach.

To verify the quality of this deformed mesh (defined as mesh morphing from NACA 0016), we also generate a mesh of the NLR 7301 airfoil directly using a hyperbolic grid generator (defined as mesh by hyperbolic grid generator). CFL3D computations for these two meshes at $M = 0.753$, AOA $= 0$ deg, and $Re = 2.0 \times 10^6$ are performed, and the results are shown in Fig. 11. Note that the C_P distributions of these two meshes are nearly identical, except at 20% chord where a slight difference occurs.

Computational Efficiency

As discussed in the third section, solving Navier's equations for large-amplitude deformations using the NBEM approach requires

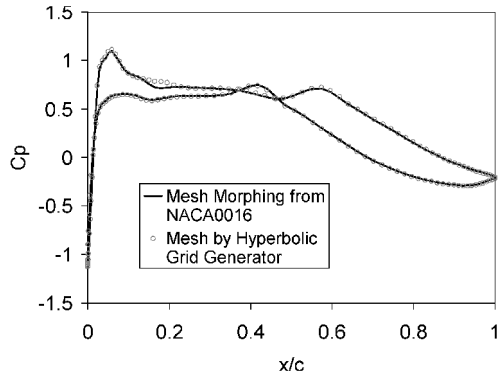

Fig. 11 Pressure distribution of NLR 7301 airfoil at Mach = 0.753, AOA = 0 deg, and $Re = 2.0 \times 10^6$.

an incremental procedure. For example, the deformed mesh of the case 1 study (NACA 0012 airfoil at 20-deg pitch-up angle at about 50% chord) is obtained by dividing the 20-deg pitch-up angle into five incremental steps, a 4-deg increment at each step. For mesh morphing or static aeroelastic analysis, such an incremental procedure is probably not computationally expensive. However, for time-marching dynamic aeroelastic simulation, the efficiency of the NBEM becomes questionable. Here, we propose two ideas as future works to improve the efficiency of NBEM; the first one is called sample points at coarse grid and the second one the modal mesh scheme.

Sample Points at Coarse Grid

The global shape function $C(x, d_n)$ shown in Eq. (19) is defined at the boundary nodes (the CFD surface mesh) and some sample points in the domain. The suggests that these sample points in the domain can be selected only at a coarse grid, rendering a reduced-size nonlinear BEM problem. Once the reduced problem is solved, the deformation at the fine grids can be analytically computed using the global shape function solution.

Modal Mesh Scheme

The idea behind the modal mesh scheme is a simple one. Dynamic aeroelastic analysis usually employs the so-called modal approach, which assumes that the displacement response can be superimposed by the natural modes of the structure, that is,

$$u_s = \sum_{i=1}^{m} \varphi_i q_i \tag{31}$$

where u_s is the displacement vector at the surface mesh defined in Eq. (4), φ_i and q_i are the natural modal vector and the generalized coordinates, respectively, and m is the number of the lower-order modes.

For dynamic aeroelastic computation involving large amplitudes, such as limit-cycle oscillations, one can usually define a largest amplitude $u_{s\max}$ as a cutoff amplitude before the computation. Beyond $u_{s\max}$, the structure may reach its failure limit and the computational result would be of little interest to the aeroelastician. This suggests that one can estimate the largest possible q_i of each mode (defined here as $q_{i\max}$), so that the resulting displacement u_s computed by Eq. (31) yields $u_{s\max}$. With $q_{i\max}$ at hand, the deformed mesh corresponding to $\varphi_i q_{i\max}$ of each mode can be computed before the aeroelastic analysis. However, this time, the deformed mesh at each incremental step, defined as the incremental modal mesh, is saved onto a database. By the use of this database, the instantaneous deformed mesh during the time-marching aeroelastic computation can be easily obtained by superimposing the interpolated deformed mesh of each mode. This interpolation is performed based on the instantaneous q_i and the incremental modal meshes retrieved from the database.

Once the modal mesh scheme is developed, NBEM becomes a preprocessor as opposed to an integral part of the CFD aeroelastic computation. This allows the aeroelastician to ensure the quality of the deforming mesh before a CFD aeroelastic simulation.

Conclusions

Numerical simulation of flow problems with moving boundaries arises in many scientific and engineering applications. These include, to name only a few, computational aeroelasticity, aerodynamic shape design/optimization, tail buffeting, and a large class of free surface problems. A robust and efficient deforming mesh methodology is one of the key elements involved in the numerical simulation of these flow problems. The TFI scheme and the spring analogy scheme can satisfy some of the deforming mesh requirements, but they lack the generality for all mesh systems, as opposed to the unified feature of the present NBEM approach.

The current CFD methods have reached their maturity for computational aeroelastic simulation, necessitating a robust and effective deforming mesh methodology. One such methodology is likely to be the present NBEM approach.

References

[1]Thomas, P. D., and Lombard, C. K., "Geometric Conservation Law and Its Application to Flow Computations on Moving Grids," *AIAA Journal*, Vol. 17, No. 10, 1979, pp. 1030–1037.

[2]Farhat, C., Lesoinne, M., and Maman, N., "Mixed Explicit/Implicit Time Integration of Coupled Aeroelastic Problems: Three-Field Formulation, Geometric Conservation and Distributed Solution," *International Journal for Numerical Methods in Fluids*, Vol. 21, No. 10, 1995, pp. 807–835.

[3]Rizzetta, D. P., and Visbal, M. R., "Comparative Numerical Study of Two Turbulence Models for Airfoil Static and Dynamic Stall," *AIAA Journal*, Vol. 31, No. 4, 1993, pp. 784–786.

[4]Krist, S. L., Biedron, R. T., and Rumsey, C. L., "CFL3D User's Manual (Version 5.0)," NASA TM-1998-208444, June 1998.

[5]Schuster, D. M., Vadyak, J., and Atta, E., "Static Aeroelastic Analysis of Fighter Aircraft Using a Three-Dimensional Navier–Stokes Algorithm," *Journal of Aircraft*, Vol. 27, No. 9, 1990, pp. 820–825.

[6]Smith, M. J., Schuster, D. M., Huttsell, L., and Buxton, B., "Development of a Euler/Navier–Stokes Aeroelastic Method for Three-Dimensional Vehicles with Multiple Flexible Surfaces," *Proceedings of the AIAA/ASME/ASCE/AHS/ASC 37th Structures, Structural Dynamics, and Materials Conference*, AIAA, Reston, VA, 1996.

[7]Guruswamy, G. P., "Unsteady Aerodynamic and Aeroelastic Calculations for Wings Using Euler Equations," *AIAA Journal*, Vol. 28, No. 3, 1990, pp. 461–469.

[8]Chen, P. C., and Jadic, I., "Interfacing of Fluid and Structural Models via an Innovative Structural Boundary Element Method," *AIAA Journal*, Vol. 36, No. 2, 1998, pp. 282–287.

[9]Chen, P. C., and Hill, L. R., "A Three-Dimensional Boundary Element Method for Computational Fluid Dynamics/CSD Grid Interfacing," AIAA Paper 99-1213, 1999.

[10]Morton, S. A., Melville, R. B., and Visbal, M. R., "Accuracy and Coupling Issues of Aeroelastic Navier–Stokes Solutions on Deforming Meshes," *Journal of Aircraft*, Vol. 35, No. 5, 1998, pp. 798–805.

[11]Batina, J. T., "Unsteady Euler Airfoil Solutions Using Unstructured Dynamic Meshes," AIAA Paper 89-0115, Jan. 1989.

[12]Farhat, C., Degand, C., Koobus, B., and Lesoinne, M., "Improved Method of Spring Analogy for Dynamic Unstructured Fluid Meshes," AIAA Paper 98-2070, April 1998.

[13]Bartels, R. E., "Mesh Strategies for Accurate Computation of Unsteady Spoiler and Aeroelastic Problems," *Journal of Aircraft*, Vol. 37, No. 3, 2000, p. 521.

[14]Banerjee, P. K., and Henry, D. P., "Advanced Applications of BEM Inelastic Analysis of Solids," *Developments in Boundary Element Methods*, Vol. 5, edited by P. K. Banerjee and R. B. Wilson, Elsevier Applied Science, London, 1989, Chap. 2.

[15]Banerjee, P. K., *The Boundary Element Methods in Engineering*, McGraw–Hill, London, 1994.

[16]Gao, X. W., and Davies, T. G., "An Effective Boundary Element Algorithm for 2D and 3D Elastoplastic Problems," *International Journal of Solids and Structures*, Vol. 37, 2000, pp. 4987–5008.

E. Livne
Associate Editor